# H$\alpha$ and Free-Free Emission from the WIM

Ruobing Dong and B. T. Draine

*Department of Astrophysical Sciences, Princeton University, Princeton, NJ, 08544*

## ABSTRACT

Recent observations have found the ratio of H$\alpha$ to free-free radio continuum to be surprisingly high in the diffuse ionized ISM (the so-called WIM), corresponding to an electron temperature of only $\sim$3000 K. Such low temperatures were unexpected in gas that was presumed to be photoionized. We consider a 3-component model for the observed diffuse emission, consisting of a mix of (1) photoionized gas, (2) gas that is recombining and cooling, and (3) cool H I gas. This model can successfully reproduce the observed intensities of free-free continuum, H$\alpha$, and collisionally-excited lines such as [N II]6583. To reproduce the low observed value of free-free to H$\alpha$, the PAH abundance in the photoionized regions must be lowered by a factor $\sim$3, and $\sim$20% of the diffuse H$\alpha$ must be reflected from dust grains, as suggested by Wood & Reynolds (1999).

*Subject headings:* atomic processes, ISM

## 1. INTRODUCTION

Low density ionized regions, often referred to as the warm ionized medium (WIM), account for $\sim$90% or more of the ionized interstellar hydrogen in the Galaxy. The WIM occupies a substantial volume fraction and is a major component of the interstellar medium (ISM) at $\sim$1 kpc above the galactic disk plane in both the Milky Way (McKee 1990; Reynolds 1991, 1993; Ferrière 2001), and in external galaxies (Rand et al. 1990; Ferguson et al. 1996; Hoopes et al. 1996; Rand 1996; Hoopes et al. 1999; Rossa & Dettmar 2000; Collins & Rand 2001). Although it is now generally believed that only massive O-type stars have enough ionizing power to account for the ionization in the WIM (Reynolds 2004), the detailed ionization mechanism is still not fully understood. Structures such as superbubbles and chimneys have been invoked to explain how H-ionizing photons could travel from the stellar sources to ionize the WIM.

Observations of optical diagnostic lines such as H$\alpha$, H$\beta$, He I$\lambda$5876, [N II]$\lambda$6548, 6583, 5755, [S II]$\lambda$6716, 6731, [O I]$\lambda$6300, [O II]$\lambda$3727, and [O III]$\lambda$5007, as well as infrared lines ([Ne II]12.81 $\mu$m and [Ne III]15.55 $\mu$m) have been made in the last two decades, aiming to understand the physical conditions in the WIM (Greenawalt et al. 1997; Rand 1997, 2000; Haffner et al. 1999; Otte et al. 2002; Miller & Veilleux 2003; Madsen et al. 2006). Although the observed line ratios vary from region to region, optical line ratios such as [N II]$\lambda$6548/H$\alpha$ appear to indicate that the WIM material has temperature $T \approx 8000 \pm 2000\,\mathrm{K}$. Hill et al. (2008) estimate the characteristic electron

density in the WIM to be $n_e \approx 0.07\mathrm{cm}^{-3}$, with a volume filling fraction of ∼30%. Optical line ratios such as [O III]$\lambda$5007/H$\alpha$ indicate that compared with H II regions powered by early O-type stars, the WIM seems to have fewer ions present that require ionization energies greater than 23 eV, with $n(\mathrm{He}^+)/n_{\mathrm{He}}$ ranging from 0.3 to 0.6 (Reynolds 1985; Rand 1997; Haffner et al. 1999; Reynolds 2004; Madsen et al. 2006; Haffner et al. 2009).

Recently, Dobler et al. (2009, hereafter DDF09), using the *WMAP* five-year data, deduced a surprisingly low temperature (∼3000 K) for the WIM from the measured ratio of the thermal bremsstrahlung (free-free) emission to the associated H$\alpha$ emission. Similar results had previously been reported based on the free-free to H$\alpha$ ratio in the *WMAP* one-year data (Davies et al. 2006) and three-year data (Dobler & Finkbeiner 2008). The low value came as a surprise, because the diffuse ionized gas had been expected to have $T \approx 8000$K, based on both observed optical line ratios and the predictions of steady-state photoionization models.

Previous discussions of the temperature and ionization of the WIM have generally assumed steady-state conditions. Here we instead argue that much of the WIM is *not* in equilibrium, and that it is possible to understand the observed line ratios and weak free-free emission if part of the WIM is assumed to be gas in the process of cooling and recombining after removal of a photoionizing source, as a consequence of either stellar evolution or changes in the opacity along the sightline between the parcel of gas and the O star providing Lyman continuum photons. We propose that observations of free-free and line emission from the diffuse ISM at high latitudes typically sum over multiple components: (1) gas currently being photoionized, (2) gas that was photoionized in the past but which is currently cooling and recombining, and (3) neutral gas (the cold neutral medium and warm neutral medium). Dust grains mixed with the gas also contribute scattered light that includes emission lines from H II regions in the disk. For plausible choices of parameters, we find that this model can account for the low ratio of free-free to H$\alpha$ found by DDF09, while also reproducing observed optical line ratios, such as [N II]6583/H$\alpha$.

The structure of this paper is as follows. In Section 2 we describe the model used to simulate cooling and recombination in the WIM. The simulation results are presented in Section 3, where we explore various factors which affect this process. In section 4 we propose a model using three ISM components to explain the observed line ratios and free-free emission. We discuss the main result and our models in Section 5, followed by a brief summary in Section 6.

## 2. Model Description

We model the evolution of temperature, ionization, and emission from cooling, recombining gas. As initial conditions we take the ionization and temperature to be consistent with photoionization by a distant OB association, but at $t = 0$ we assume that the radiation with $h\nu > 13.6$ eV is suddenly turned off. The remaining ionization and heating sources are cosmic rays and photoelectric emission by the diffuse interstellar radiation field with $h\nu < 13.6$ eV. We follow the ionization of 11 elements:

H, He, C, N, O, Ne, Mg, Si, S, Ar, and Fe, which includes all the elements that normally have gas phase abundance relative to H above $10^{-6}$, and includes all important coolants.

### 2.1. Physics in the Model

The evolution is assumed to take place at constant volume, with H nucleon density $n_{\rm H} = const.$ The abundance $x_{A,r} \equiv n(A^{+r})/n_{\rm H}$ of ion $A^{+r}$ evolves according to

$$\begin{aligned} \frac{dx_{A,r}}{dt} &= \zeta_{A,r-1}x_{A,r-1} + \left[n_e\left(\alpha_{A,r+1}^{(rr)} + \alpha_{A,r+1}^{(dr)}\right) + n_{\rm H}\alpha_{A,r+1}^{(gr)}\right]x_{A,r+1} \\ &\quad - \left[\zeta_{A,r} + n_e\left(\alpha_{A,r}^{(rr)} + \alpha_{A,r}^{(dr)}\right) + n_{\rm H}\alpha_{A,r}^{(gr)}\right]x_{A,r} \qquad \text{for } r \geq 1 \ , \qquad (1) \\ \frac{dx_{A,0}}{dt} &= \left[n_e\left(\alpha_{A,1}^{(rr)} + \alpha_{A,1}^{(de)}\right) + n_{\rm H}\alpha_{A,1}^{(gr)}\right]x_{A,1} - \zeta_{A,0}x_{A,0} \quad , \qquad (2) \end{aligned}$$

where $\zeta_{A,r}$ is the probability per unit time of ionization $A^{+r} \rightarrow A^{+r+1} + e^-$ due to either photoionization, cosmic rays, or secondary electrons; $\alpha_{A,r}^{(rr)}$ is the rate coefficient for radiative recombination; $\alpha_{A,r}^{(dr)}$ is the rate coefficient for dielectronic recombination; and $\alpha_{A,r}^{(gr)}$ is the effective rate coefficient for recombination on dust grains. The present model includes only ions with $r \leq 2$, and gas temperatures $T \leq 10^4\,{\rm K}$. We assume case B recombination for H and He. The recombination rate for H is taken to be (Draine 2011)

$$\alpha_B = 2.54 \times 10^{-13} T_4^{-0.8163-0.0208\ln T_4}\,{\rm cm^3\,s^{-1}} \quad , \qquad (3)$$

where $T_4 \equiv T/10^4{\rm K}$, and for recombination of He II→He I we take

$$\alpha_B({\rm He}) = 2.72 \times 10^{-13} T_4^{-0.789}\,{\rm cm^3\,s^{-1}} \quad . \qquad (4)$$

For other elements, radiative recombination rates are evaluated by subroutine rrfit.f from Verner (1999), which uses rates from Pequignot et al. (1991) for ions of C, N, O, and Ne (refitted with the formula of Verner & Ferland (1996)), and from Shull & van Steenberg (1982) for ions of Mg, Si, S, Ar, and Fe. Rate coefficients $\alpha^{(dr)}$ for Mg and Si were from Nussbaumer & Storey (1986), for S were from Shull & van Steenberg (1982), and for Fe were from Arnaud & Raymond (1992). Rate coefficients $\alpha_{A,r}^{(gr)}$ for recombination on grains are taken from Weingartner & Draine (2001a). The electron density $n_e \equiv n_{\rm H}\sum_A\sum_r r x_{A,r}$, and the free particle density $n = n_e + n_{\rm H}\sum_A\sum_r x_{A,r}$.

For isochoric evolution, the temperature $T$ evolves according to

$$\frac{dT}{dt} = \frac{\Gamma - \Lambda}{(3/2)nk} - T\frac{1}{n}\frac{dn}{dt} \quad , \qquad (5)$$

where $(\Gamma - \Lambda)$ is the net rate of change of thermal kinetic energy per unit volume due to heating and cooling processes (including ionization and recombination), and $dn/dt$ is the net rate of change of the free particle density due to ionization and recombination processes. The heating rate per

volume $\Gamma$ includes heat deposition by cosmic ray ionization and by photoelectrons emitted from atoms, ions, and grains. The cooling rate per volume $\Lambda$ includes kinetic energy removed from the gas by inelastic collisions and by recombination of ions and electrons. The mean kinetic energy per recombining electron is taken to be (Draine 2011, eq. 27.23)

$$\langle E_{\rm rr}\rangle \approx [0.684 - 0.0416 \ln T_4]\, kT \quad . \tag{6}$$

Radiative cooling processes consist of free-free emission, and line emission following collisional excitation of various atoms and ions. Collisional deexcitation is included, although it is unimportant at the densities considered here.

Grain-related processes are included in our simulation. From their study of the "spinning dust" emission from the WIM, DDF09 concluded that the PAH abundance in the WIM is a factor $\sim$3 lower than in the H I. Because the PAHs account for a large fraction of the photoelectric heating (Bakes & Tielens 1994; Weingartner & Draine 2001b), and are also thought to dominate the grain-assisted recombination (Weingartner & Draine 2001a), depletion of the PAHs will affect the heating and recombination. To explore this, we multiply the rates for dust photoelectric heating and grain-assisted recombination by a factor $g$, where $g = 1$ gives the rates estimated for normal grain abundances in the diffuse ISM for photoelectric heating and grain-assisted recombination (Weingartner & Draine 2001a). Our standard model for the WIM assumes $g = 1/3$, which presumably results primarily from reduced abundances of the small grains that account for most of the grain surface area. We will explore the sensitivity to the reduction factor $g$ by also performing simulations with $g = 1$ (no reduction in PAH abundance) and $g = 0.1$, a factor of 10 suppression of grain photoelectric heating and grain-assisted recombination. Grain photoelectric heating is calculated following Weingartner & Draine (2001b), and the $g = 1$ rates for grain-assisted recombination are taken from Weingartner & Draine (2001a).

We calculate collisional excitation and resulting radiative cooling by ions of C, N, O, Ne, Si, S, Ar, and Fe. We include a total of 159 lines, but the 26 lines of listed in Table 1 account for more than 95% of the radiative cooling at each point in the thermal evolution of our models. Sources of the collisional rate coefficients for species used in our calculations are listed in Table 2.

Table 1: Principal Cooling Lines (wavelengths *in vacuo*)

| | | | |
|---|---|---|---|
| [C II]157.7$\mu$m | [O I]145.5$\mu$m | [S II]6733Å | [Fe II]25.99$\mu$m |
| [C II]2328Å | [O I]63.19$\mu$m | [S II]6718Å | [Fe II]5.340$\mu$m |
| [C II]2326Å | [O I]6302Å | [S II]4070Å | [Fe II]1.644$\mu$m |
| [N II]205.3$\mu$m | [O II]3730Å | [S III]33.48$\mu$m | [Fe II]1.321$\mu$m |
| [N II]121.8$\mu$m | [O II]3727Å | [S III]18.71$\mu$m | [Fe II]1.257$\mu$m |
| [N II]6585Å | [Ne II]12.81$\mu$m | [S III]9533Å | |
| [N II]6550Å | [Si II]34.81$\mu$m | [S III]9071Å | |

Table 2: Sources for Collisional Rate Coefficients

| Ion | Transition | $e^-$ | $H^0$ |
|---|---|---|---|
| C II | $^2P^o_{1/2} - {}^2P^o_{3/2}$ | Tayal (2008) | Barinovs et al. (2005) |
| N II | $^3P_J - {}^3P_{J'}$ | Hudson & Bell (2005) | — |
| N II | $^3P_J - {}^1D_2$ | Hudson & Bell (2005) | — |
| O I | $^3P_J - {}^3P_{J'}$ | Pequignot (1996) | Abrahamsson et al. (2007) |
| O I | $^3P_J - {}^1D_2$ | Pequignot (1996) | — |
| O II | $^4S^o_{3/2} - {}^2D^o_J$ | Tayal (2007) | — |
| Ne II | $^2P^o_{3/2} - {}^2P^o_{1/2}$ | Griffin et al. (2001) | — |
| Si II | $^2P^o_{1/2} - {}^2P^o_{3/2}$ | Bautista et al. (2009) | — |
| S II | $^4S^o_{3/2} - {}^2D^o_J$ | Tayal & Zatsarinny (2010) | Barinovs et al. (2005) |
| S III | $^3P_J - {}^3P_{J'}$ | Tayal & Gupta (1999) | — |
| S III | $^3P_J - {}^1D_2$ | Tayal & Gupta (1999) | — |
| Fe II | $^6D_J - {}^6D_{J'}$ | Ramsbottom et al. (2007) | — |
| Fe II | $^6D_J - {}^4F_{J'}$ | Ramsbottom et al. (2007) | — |
| Fe II | $^6D_J - {}^4D_{J'}$ | Ramsbottom et al. (2007) | — |

For the diffuse interstellar radiation field we use the estimate of Mathis et al. (1983). Photoionization rates for this radiation field were taken from Draine (2011, Table 13.1), calculated using photoionization cross sections from Verner & Yakovlev (1995) and Verner et al. (1996).

We include secondary ionization and heating by cosmic rays following Dalgarno & McCray (1972). Charge exchange between H and O is included in our model, with rate coefficients from Stancil et al. (1999).

### 2.2. Free-Free vs. H$\alpha$

We calculate the free-free emission at 41 GHz, $I_\nu(41\,\mathrm{GHz})$, to compare with observations (DDF09):

$$j_\nu = 5.44 \times 10^{-41} g_{\rm ff} T_4^{-0.5} \mathrm{e}^{-h\nu/kT} n_e^2 \text{ erg cm}^3 \text{ s}^{-1} \text{ Hz}^{-1} \text{ sr}^{-1}. \quad (7)$$

where $n_e$ is the electron number density, and the Gaunt factor (Hummer 1988) is accurately approximated by (Draine 2011, eq. 10.9)

$$g_{\rm ff} \approx \ln\left[\exp\left(5.96 - \frac{\sqrt{3}}{\pi}\ln(\nu_9 T_4^{-1.5})\right) + \mathrm{e}\right] \quad . \quad (8)$$

where $\nu_9 \equiv \nu/\mathrm{GHz}$. The H$\alpha$ emission rate is:

$$j_{\mathrm{H}\alpha} = 2.82 \times 10^{-26} T_4^{-0.942-0.031\ln(T_4)} n_e n(\mathrm{H}^+) \text{ erg cm}^3 \text{ s}^{-1} \text{ sr}^{-1} \quad . \quad (9)$$

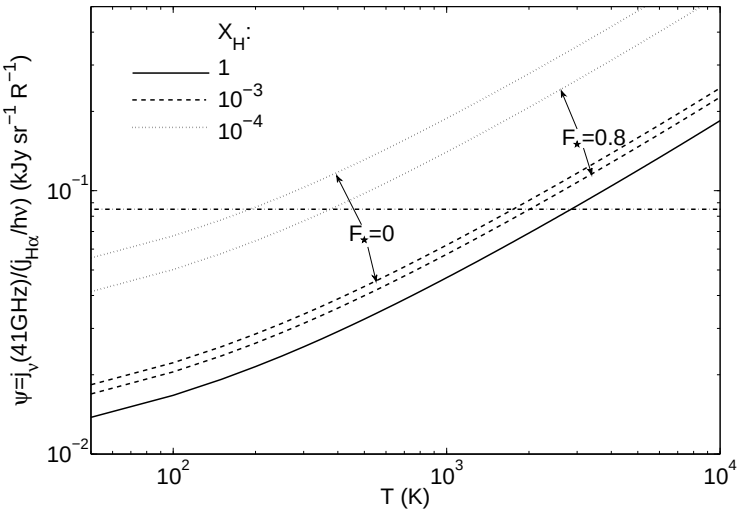


Fig. 1.— The ratio of $j_\nu(41\mathrm{GHz})/(\mathrm{j_{H\alpha}/h\nu})$ as a function of gas temperature $T$ for H ionization fraction $x_\mathrm{H} = 1$ (solid curve), $10^{-3}$ (dash curves), and $10^{-4}$ (dot curves). For each $x_\mathrm{H}$, upper curves employ gas phase elemental abundances for $F_\star = 0$ to simulate WIM, lower curves employ gas phase elemental abundances for $F_\star = 0.8$ to simulate CNM. Observed nearly all-sky averaged free-free/H$\alpha$ ratio $\sim 0.85\,\mathrm{kJy\,sr^{-1}\,R^{-1}}$ from *WMAP* (DDF09) is indicated by the horizontal dash-dot line, corresponding to gas temperature ∼3000 K for fully ionized gas.

corresponding to an effective rate coefficient

$$\alpha_{\mathrm{H}\alpha} \equiv \frac{4\pi j_{\mathrm{H}\alpha}}{h\nu} = 1.17\times 10^{-13} T_4^{-0.942-0.031\ln(T_4)}\,\mathrm{cm^3\,s^{-1}} \quad . \tag{10}$$

The ratio of free-free to H$\alpha$ depends on both the temperature and the fraction of the electrons contributed by $\mathrm{H^+}$:

$$\begin{aligned}\psi(T) &\equiv \frac{j_\nu(41\,\mathrm{GHz})}{j_{\mathrm{H}\alpha}/h\nu} \\ &\approx 0.0465\frac{n_e}{n(\mathrm{H^+})} T_4^{0.442+0.031\ln T_4} \ln\left[\exp\left(3.913+\frac{3\sqrt{3}}{2\pi}\ln T_4\right)+\mathrm{e}\right]\frac{\mathrm{kJy\ sr^{-1}}}{\mathrm{R}} \quad .\end{aligned} \tag{11}$$

Free-free emission comes from all ions, therefore in low-ionization gas we have free-free emission from ions such as $\mathrm{C^+} + e^-$, whereas H$\alpha$ comes only from $\mathrm{H^+} + e^-$. Therefore, if H becomes almost neutral, $\psi$ is sensitive to the gas-phase abundance of elements that can be ionized by $h\nu < 13.6$ eV photons. Figure 1 shows $\psi(T)$ as a function of gas temperature from $50 - 10^4$ K, for three different H ionization fractions $x_\mathrm{H} \equiv n(\mathrm{H^+})/\mathrm{n_H}$: $x_\mathrm{H} = 1$ (solid curve), $10^{-3}$ (dash curves) and $10^{-4}$ (dot curves), and for two gas phase elemental abundances: $F_\star = 0$, representing WIM, and $F_\star = 0.8$, representing CNM. The horizontal dash-dot line indicates the observed free-free/H$\alpha$ ratio $\sim 0.085\,\mathrm{kJy\,sr^{-1}\,R^{-1}}$ determined from the *WMAP* 5 year data (DDF09). The observed ratio corresponds to gas temperature ∼3000 K for fully ionized hydrogen.

In addition to emission from the WIM, there will be some H$\alpha$ and free-free emission from H I clouds. The H I gas in the interstellar medium is found at a wide range of temperatures. The

majority is in the CNM phase, at $T \approx 10^2$ K, with $n_e/n(\mathrm{H}^+) \approx 2$ (if $\zeta_{\rm CR}/n(\mathrm{H}) \sim 2 \times 10^{-16} \mathrm{cm}^3 \mathrm{s}^{-1}$, then ∼50% of the free electrons are from $\mathrm{C}^+$, $\mathrm{S}^+$, and other metal ions.) From this gas we expect $\psi \approx 0.017 [n_e/n(\mathrm{H}^+)]\,\mathrm{kJy\,sr^{-1}\,R^{-1}} \approx 0.034\,\mathrm{kJy\,sr^{-1}\,R^{-1}}$. In addition, a substantial fraction of the H I is in the WNM phase, with $T \approx 10^3$ K; this gas will have $\psi \approx 0.047\,\mathrm{kJy\,sr^{-1}\,R^{-1}}$. Overall, we estimate that the H$\alpha$ and free-free emission from the H I phase will have $\psi_{\rm H\,I} \approx 0.04$.

### 2.3. Initial Conditions

Gas-phase elemental abundances are based on the recent study by Jenkins (2009). For our standard model, we use abundances from the model of Jenkins (2009) with $F_\star = 0$, representing a relatively low level of depletion (see Section 5 for a discussion of the choice of $F_\star$). For Ne and Ar (not covered in Jenkins' study), we assume solar abundances from Asplund et al. (2009). He/H=0.1 is also assumed. In addition, we construct a model with $F_\star = 0.25$ (reduced gas phase abundance for elements that deplete) to explore the sensitivity to coolant abundances. Carbon requires special attention, since recent work (Sofia & Parvathi 2010) indicates that the oscillator strength of C II]2325Å is larger than previously estimated, implying that gas phase C abundances estimated from measurements of C II]2325Å could be lowered by a factor ∼2. For this reason, in addition to the standard model and the $F_\star = 0.25$ model, we consider the "Reduced C" model in which C has an abundance two thirds of its $F_\star = 0$ value and other elements all have their $F_\star = 0$ values.

For our standard model we take $n_{\rm H} = 0.5\,\mathrm{cm}^{-3}$ and initial temperature $T_i = 8000$ K. Under these conditions the thermal pressure of the photoionized state, $p/k \approx 2.15 n_{\rm H} T \approx 9 \times 10^3\,\mathrm{cm}^{-3}\,\mathrm{K}$, is comparable to, although somewhat higher than, current estimates for pressures in the diffuse ISM. In our standard model, the initial ionization fractions (IIF) of all the elements (Table 3) are adopted from Sembach et al. (2000), where we use the value in their standard model with parameter $\chi_{\rm edge} = 0.1$ for fully ionized gas (Sembach et al. 2000, Table 5), corresponding to a fairly soft ionization field. Two other IIFs (Table 3) considered include values from the Orion nebula (Baldwin et al. 1991), which corresponds to a hard radiation field, and a set of observed values based on various previous studies of the WIM (Haffner et al. 1999; Reynolds 2004; Madsen et al. 2006; Haffner et al. 2009). The effects of initial gas density and temperature are studied as well. Table 4 summarizes all the models in our simulations.

The cosmic ray primary ionization rate for an H atom, $\zeta_{\rm CR}$, is controversial. Direct measurement of the cosmic ray flux (Wang et al. 2002) at $E \lesssim 1\,\mathrm{GeV}$ is affected by the solar wind. Webber & Yushak (1983) attempted to correct for solar wind modulation. Smoothly extrapolating the Webber & Yushak (1983) spectrum to lower energy suggests $\zeta_{\rm CR} \sim 1.3 \times 10^{-17}$ s$^{-1}$. However, studies of the ionization conditions inside molecular clouds (Black & van Dishoeck 1991; Lepp 1992; McCall et al. 2003; Indriolo et al. 2007) indicate primary ionization rates $\zeta_{\rm CR} \sim 0.3 - 3 \times 10^{-16}$ s$^{-1}$, and we will consider values of $\zeta_{\rm CR}$ within this range. We adopt $\zeta_{\rm CR} = 1 \times 10^{-16}$ s$^{-1}$ for the standard model, and will then explore varying $\zeta_{\rm CR}$ from $2 \times 10^{-17}$ s$^{-1}$ to $5 \times 10^{-16}$ s$^{-1}$.

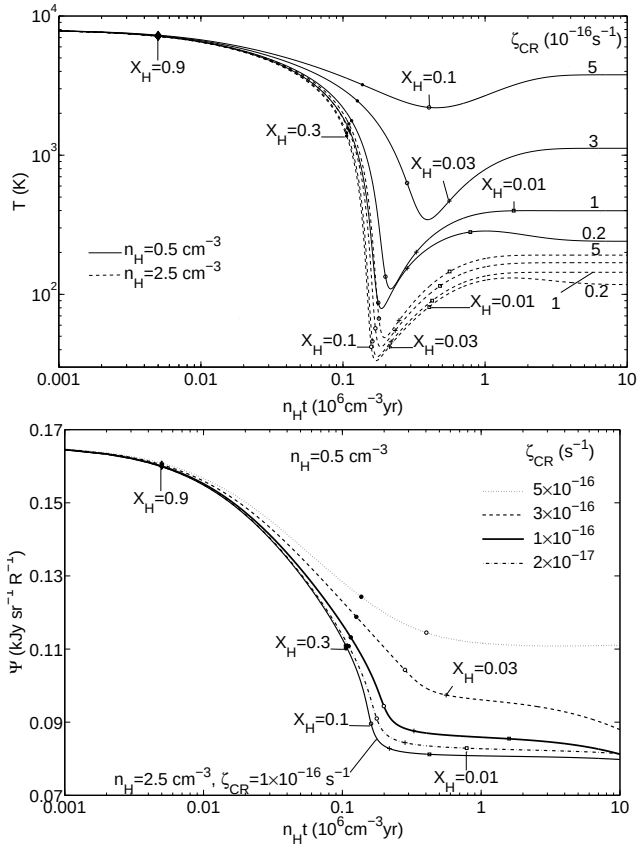


Fig. 2.— Effect of different density and cosmic ray ionization rate. All cases have $g = 1/3$ and $F_\star = 0$. Top panel: The temperature evolution for $n_{\rm H} = 0.5$ cm$^{-3}$ (solid curves) and $n_{\rm H} = 2.5$ cm$^{-3}$ (dashed curves), and different cosmic ray ionization rate $\zeta_{\rm CR}$. Bottom panel: The ratio of cumulative free-free emission at 41 GHz to cumulative H$\alpha$ emission for models with different $\zeta_{\rm CR}$ for $n_{\rm H} = 0.5$ cm$^{-3}$. Values of $x_{\rm H} = n({\rm H}^+)/{\rm n_H}$ are given at several points along the curves by different tick marks. Note that when $\zeta_{\rm CR}/n_{\rm H} > 6 \times 10^{-16}$ cm$^3$s$^{-1}$, the final temperature $T_f > 10^3$K, and $\Phi(n_{\rm H}t = 10^7\,{\rm cm^{-3}\,yr}) > 0.09\,{\rm kJy\,sr^{-1}\,R^{-1}}$.

## 3. Results

The temperature as a function of time for our standard model is shown in the top panel of Figure 2. Initially the gas cools rapidly, reaches a minimum temperature ∼100 K within 0.4 Myr, and then warms up to 400 K, approaching its asymptotic state in several Myr. The rise in temperature at $n_{\rm H}t \gtrsim 2 \times 10^5\,{\rm cm^{-3}\,yr}$ occurs because the [C II]158$\mu$m cooling declines as free electrons recombine. Similar late time reheating has been seen previously (e.g., Draine 1978). Define the cumulative emission ratio as:

$$\Psi(t) \equiv \frac{\int_0^t j_\nu(41\,{\rm GHz})dt'}{\int_0^t (j_{\rm H\alpha}/h\nu)dt'} \quad ; \tag{12}$$

$\Psi$ starts from ∼0.17 kJy sr$^{-1}$ R$^{-1}$, corresponding to the initial temperature $T_i = 8000$ K, then drops as the gas cools, to ∼0.08 for $10^6{\rm cm^{-3}\,yr} \lesssim n_{\rm H}t \lesssim 10^7{\rm cm^{-3}\,yr}$ as shown in the bottom panel of Figure 2. This low value of $\Psi$ is consistent with the observed value of $\sim 0.085\,{\rm kJy\,sr^{-1}\,R^{-1}}$

(DDF09).

Altering the parameters in the standard model will change the cooling history, and we explore the influence of various factors. Based on their impact, we divide the influential factors into two classes: major factors, which includes $\zeta_{\rm CR}$, $n_{\rm H}$, abundance of metal elements and grain depletion, and minor factors: the initial temperature and IIF.

### 3.1. Major factors

Figure 2 shows the sensitivity to $\zeta_{\rm CR}$ and $n_{\rm H}$. For fixed $n_{\rm H}$, the final asymptotic temperature ($T_f$) increases with increasing cosmic ray ionization rate, while for fixed $\zeta_{\rm CR}$, $T_f$ decreases with increasing $n_{\rm H}$. At a higher density the final temperature and free-free to H$\alpha$ emission ratio become less sensitive to $\zeta_{\rm CR}$. For $\zeta_{\rm CR}$ ranging from $2 \times 10^{-17}$ s$^{-1}$ to $5 \times 10^{-16}$ s$^{-1}$, $T_f$ increases from $\sim$240 K to $\sim$3800 K when $n_{\rm H} = 0.5$ cm$^{-3}$, but only from 120 K to 190 K when $n_{\rm H} = 2.5$ cm$^{-3}$ (as shown in top panel of Figure 2). As $\zeta_{\rm CR}$ is varied from $2 \times 10^{-17}$ to $5 \times 10^{-16}$ s$^{-1}$, the emission ratio $\Psi(n_{\rm H}t = 10^7\,{\rm cm}^{-3}\,{\rm yr})$ changes about 20% for $n_{\rm H} = 0.5$ cm$^{-3}$ (as shown in bottom panel of Figure 2), but only about 1% for $n_{\rm H} = 2.5$ cm$^{-3}$. For each density, there is a critical value of $\zeta_{\rm CR}$, above which the gas remains warm, with asymptotic temperature $T > 3000$K, and $\Psi > 0.10$.

Elemental abundances affect the cooling process. Figure 3 shows the effect of varying the element abundances. In general, reducing gas phase abundances will reduce the cooling, increase the final temperature $T_f$, and consequently will raise $\Psi$. As we discussed in Section 2.1, evidence from analyzing spinning dust emission in the WIM (DDF09) suggests that the small polycyclic aromatic hydrocarbons (PAHs) may be underabundant in the WIM relative to the general ISM. We explore the effect of different grain reduction factors, with $g = 1/3$ as our standard model. As shown in Figure 3, the final value of $\Psi$ is quite sensitive to the value of the PAH reduction factor $g$. When $g$ is reduced, the photoelectric heating rate drops; since the grain-assisted recombination rate also drops, more electrons and ions will be present in the gas phase, leading to increased cooling through collisionally-excited lines. The combined result of the two factors is that the ionized gas recombines more slowly, cools faster, and reaches lower values of $\Psi$ when $g$ is small.

### 3.2. Minor factors

The initial temperature and ionization fractions also affect the cooling process. Quantities like $T$ and $x_{\rm H}$ for models with different initial $T$ and ionization will evolve differently at the initial stage of the simulations, but will all converge to the same asymptotic steady-state values. On the other hand, the cumulative ratio of free-free to H$\alpha$, $\Psi$, will differ because it involves integration over time. We study the effect of different $T_i$ by running a model with $T_i = 10^4$ K (instead of 8000 K), and we study the effect of different IIF by running models with IIF2 and IIF3. IIF3 assumes Orion Nebula values (Baldwin et al. 1991), formed by a much harder ionization field than

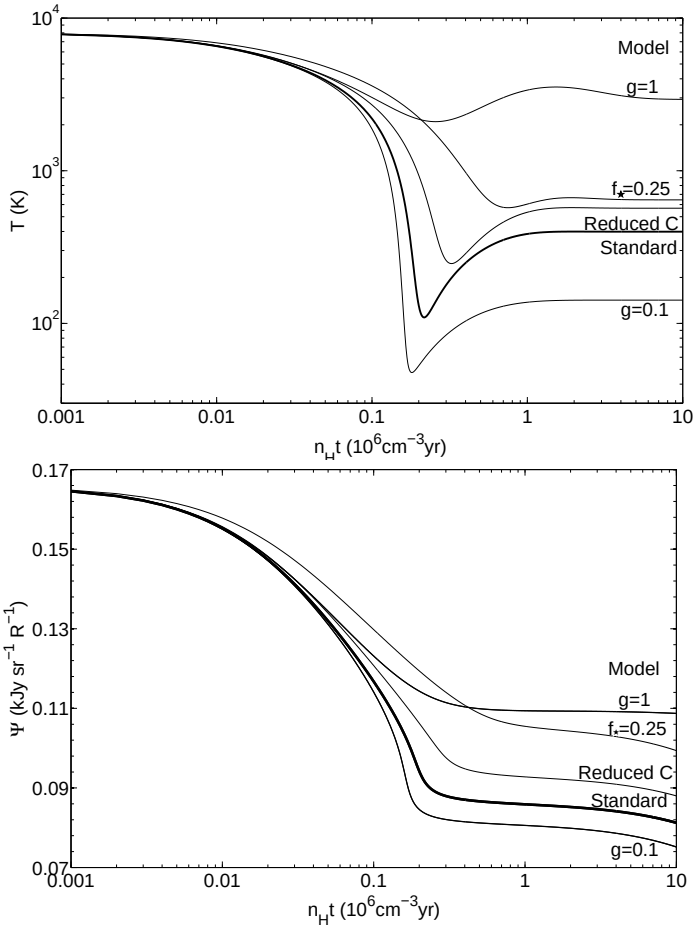


Fig. 3.— Effect of varying gas-phase abundances ($F_\star = 0.25$ vs. $F_\star = 0$), PAH abundance ($g = 1$ vs. $g = 1/3$), and C abundance (Reduced C vs. $F_\star = 0$). Top panel shows the temperature as a function of time for different models (indicated by model name), and bottom panel show the ratio of cumulative free-free emission at 41 GHz to cumulative H$\alpha$ emission as a function of time.

the one that forms the WIM, as we discussed above in Section 1. IIF2 is a set of values based on the literature (Madsen et al. 2006; Haffner et al. 1999, 2009; Reynolds 2004), falling between IIF3 and our standard model. These three models cover a large range of IIF. As shown in Figure 4, the results are insensitive to changes in the different initial ionization conditions.

## 4. A Three Component Model for the Diffuse Emission

In this section we try to compose a model to simultaneously explain the observed low free-free to H$\alpha$ emission ratio (corresponding to $T \sim 3000$ K), and line ratios such as [N II]$\lambda$6583/H$\alpha$ and [N II]$\lambda$5755/[N II]$\lambda$6583 (indicating $T \gtrsim 8000\,$K) in the diffuse emission from the WIM. We note that the observed low free-free to H$\alpha$ emission ratio (DDF09) comes from measurements which integrate over a large fraction of the high-latitude sky, while the measurement of various other diagnostic

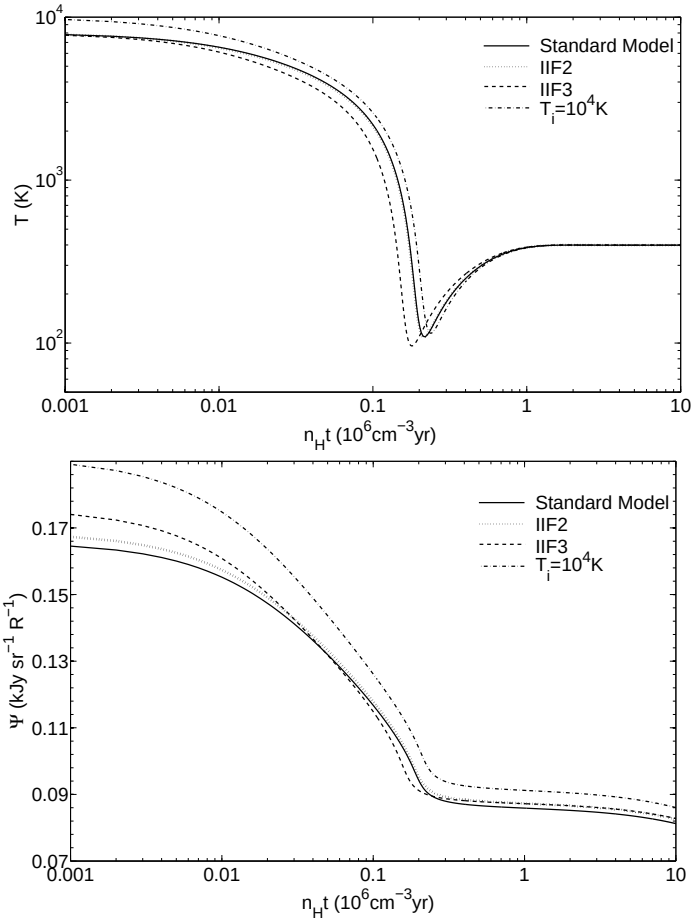


Fig. 4.— Effect of different initial conditions (initial temperature and ionization fractions) on the evolution of temperature $T$ and the cumulative ratio $\Psi$ of 41 GHz free-free to H$\alpha$.

lines from the WIM, like [N II]$\lambda$6583 or [N II]$\lambda$5755, are limited to relatively high intensity regions.

In our model, the observed diffuse emission comes from three components:

1. "hot"photoionized gas with $T \approx 10^4$K, nearly fully ionized, producing free-free emission, recombination radiation, and collisionally-excited lines such as [N II]$\lambda$6583 and [N II]$\lambda$5755;

2. cooling and recombining gas, which starts from the "hot" photoionized phase and cools and recombines to give H$\alpha$ and free-free emission as well as a small amount of collisionally-excited lines, such as [N II]$\lambda$6583;

3. neutral H I gas, partially in the "cold neutral medium"(CNM), with $T \approx 10^2$K, and partially in the "warm neutral medium" (WNM), with $T \approx 10^3$ K; together these emit a small amount of H$\alpha$ and free-free emission due to cosmic ray ionization, but negligible metal line emission in the optical.

In addition to the actual emission from the H I gas, there will also be reflected light – both H$\alpha$ and metal lines such as [N II]$\lambda$6583 – that was originally emitted elsewhere, mainly regular H II regions, and then reflected by dust grains present in the H I gas. Let $f_{\rm H\alpha}^{\rm (refl)}$ be the fraction of the observed H$\alpha$ that is scattered light. Wood & Reynolds (1999) estimated that $f_{\rm H\alpha}^{\rm (refl)} \approx 0.05 - 0.20$ at high galactic latitudes. In our calculation, we assume the reflection coefficients of [N II]$\lambda$6583, [N II]$\lambda$5755 and [S II]$\lambda$6716 are the same as H$\alpha$, because the wavelengths are close to H$\alpha$.

The observed intensities are weighted averages over the three components. Here we ask what weighting factors are needed to reproduce the observed low ratio of free-free/H$\alpha$, as well as other line ratios.

The relative contributions of the three components can be determined from the observed emission ratios. Among all the diagnostic line ratios in the WIM, [N II]$\lambda$6583/H$\alpha$ and [S II]$\lambda$6716/H$\alpha$ are the two best-studied cases, while other lines have been studied only in a few select directions (Haffner et al. 2009). These two line ratios depend on temperature and ionization fraction of N and S in the gas. The high second ionization potential of N (29.60 eV) protects it from being doubly ionized in the WIM, which has a generally soft ionization field (Madsen et al. 2006). This factor along with the similar first ionization potentials of N and H (14.53 and 13.60 eV) make $\rm N^+/N$ close to unity in the H II gas (Madsen et al. 2006; Haffner et al. 1999). On the other hand, some of the S in H II regions will be doubly ionized due to its low second ionization potential (23.33 eV), which leads to uncertainty in the predicted [S II]$\lambda$6716/H$\alpha$, reducing the utility of [S II]$\lambda$6716/H$\alpha$ as a constraint. Nevertheless, we have calculated the integrated value of [S II]$\lambda$6716/H$\alpha$ for the cooling gas (see Table 4).

Let $f_{\rm H\alpha}^{\rm (hot)}$ and $f_{\rm H\alpha}^{\rm (H\,I)}$ be, respectively, the fraction of the observed diffuse H$\alpha$ emitted from the photoionized gas and H I clouds, and let $f_{\rm H\alpha}^{\rm (refl)}$ be the fraction of the observed H$\alpha$ that is actually reflected from dust in H I. Then $f_{\rm H\alpha}^{\rm (cooling)} = 1 - f_{\rm H\alpha}^{\rm (hot)} - f_{\rm H\alpha}^{\rm (H\,I)} - f_{\rm H\alpha}^{\rm (refl)}$ is the fractional contribution of the cooling material. The emission from this three component model depends on four parameters: $f_{\rm H\alpha}^{\rm (hot)}$, $f_{\rm H\alpha}^{\rm (H\,I)}$, $f_{\rm H\alpha}^{\rm (refl)}$, and the temperature $T_{\rm hot}$ of the photoionized component. For an adopted value of $f_{\rm H\alpha}^{\rm (refl)}$, a physical solution must have $0 \le f_{\rm H\alpha}^{\rm (hot)} \le 1 - f_{\rm H\alpha}^{\rm (refl)}$, $0 \le f_{\rm H\alpha}^{\rm (cooling)} \le 1 - f_{\rm H\alpha}^{\rm (refl)}$, and $0 \le f_{\rm H\alpha}^{\rm (H\,I)} \le 1 - f_{\rm H\alpha}^{\rm (refl)}$. We take the observed free-free/H$\alpha$ and [N II]$\lambda$6583/H$\alpha$ emission ratios as two constraints to solve for the relative fraction of the three components.

The instantaneous [N II]$\lambda$6583/H$\alpha$ line ratio is:

$$\phi(T) \equiv \frac{j_{\rm [NII]\lambda6583}}{j_{\rm H\alpha}} \approx 12.4\ T_4^{0.495+0.040\ln T_4}\ {\rm e}^{-2.204/T_4}\,\frac{n({\rm N^+})/n({\rm H^+})}{7.41\times10^{-5}} \quad . \tag{13}$$

where we use the collision strength $\Omega(^3P_0,{}^1D_2) = 0.303T_4^{0.0528+0.009\ln T_4}$ from Hudson & Bell (2005). The cumulative ratio of [NII]6583 to H$\alpha$ for cooling gas is

$$\Phi(t) \equiv \frac{\int_0^t j_{\rm [NII]6583}\,dt'}{\int_0^t j_{\rm H\alpha}\,dt'} = \frac{\int_0^t \phi(t')\,j_{\rm H\alpha}\,dt'}{\int j_{\rm H\alpha}\,dt'} \quad . \tag{14}$$

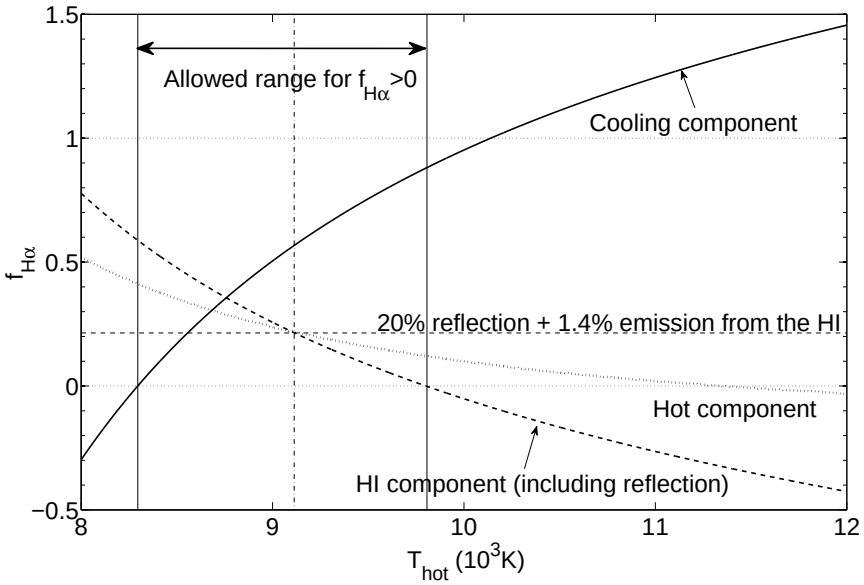


Fig. 5.— H$\alpha$ fractions for the three gas components based on two constraints ($I_\nu(41\,\mathrm{GHz})/\mathrm{H}\alpha = 0.85\,\mathrm{kJy\,sr^{-1}R^{-1}}$ and [N II]$\lambda$6583/H$\alpha$=0.4), as a function of hot (photoionized) gas temperature $T_{\rm hot}$. The equations are solved under these assumptions: $f_{\mathrm{H}\alpha}^{(\mathrm{refl})} = 0.20$, $f_{\mathrm{H}\alpha}^{(\mathrm{H\,I})} = 0.014$, $n(\mathrm{H}^+)/n_e = 0.5$ in the H I (corresponding to $\zeta_{\rm CR} \sim 1\times10^{-16}\mathrm{s}^{-1}$ in CNM), and $\mathrm{He}^+/\mathrm{He}$=0.3 in the hot ionized gas, as in IIF1. The fact that $f_{\mathrm{H}\alpha}^{(\mathrm{refl})} + f_{\mathrm{H}\alpha}^{(\mathrm{H\,I})} \approx f_{\mathrm{H}\alpha}^{(\mathrm{hot})}$ is coincidental.

Cooling gas in our standard model gives $\Phi \approx 0.06$ (see Table 4). The WNM and CNM contribute negligible [N II]$\lambda$6583.

We take the average value of [N II]6583/H$\alpha$ = 0.4, based on observations (Reynolds 2004; Reynolds et al. 2001; Madsen et al. 2006). Then we must have

$$0.4 = (f_{\mathrm{H}\alpha}^{(\mathrm{hot})} + f_{\mathrm{H}\alpha}^{(\mathrm{refl})})\phi(T_{\rm hot}) + (1 - f_{\mathrm{H}\alpha}^{(\mathrm{hot})} - f_{\mathrm{H}\alpha}^{(\mathrm{H\,I})} - f_{\mathrm{H}\alpha}^{(\mathrm{refl})})\Phi \quad . \tag{15}$$

Note that in this equation, we assume the reflected component has the same [N II]$\lambda$6583/H$\alpha$ ratio as the hot ionized component, as discussed previously.

The ratio of all-sky free-free to H$\alpha$ emission is $I_\nu(41\,\mathrm{GHz})/I(\mathrm{H}\alpha) \sim 0.085$ kJy sr$^{-1}$ R$^{-1}$ (DDF09). Thus we must have

$$0.085\,\mathrm{kJy\,sr^{-1}\,R^{-1}} = f_{\mathrm{H}\alpha}^{(\mathrm{hot})}\psi(T_{\rm hot}) + (1 - f_{\mathrm{H}\alpha}^{(\mathrm{hot})} - f_{\mathrm{H}\alpha}^{(\mathrm{H\,I})} - f_{\mathrm{H}\alpha}^{(\mathrm{refl})})\Psi + f_{\mathrm{H}\alpha}^{(\mathrm{H\,I})}\psi_{\mathrm{H\,I}} \quad . \tag{16}$$

For trial values of $T_{\rm hot}$ and $f_{\mathrm{H}\alpha}^{(\mathrm{refl})} \geq 0$, we can use the observed $I([\mathrm{N\,II}]6583)/I(\mathrm{H}\alpha)$ and $I_\nu(41\mathrm{GHz})/I(\mathrm{H}\alpha)$ to determine $f_{\mathrm{H}\alpha}^{(\mathrm{hot})}$ and $f_{\mathrm{H}\alpha}^{(\mathrm{H\,I})}$, by solving the two linear equations (15) and (16). The coefficients $\psi(T_{\rm hot})$ and $\phi(T_{\rm hot})$ are obtained from eq. (11) and (13), while $\Psi \approx 0.08$ and $\Phi \approx 0.06$ are obtained from the appropriate simulations as their asymptotic values (see Table 4 as well as Figure 2). Based on the discussion in §2.2, we take $\psi_{\mathrm{H\,I}} \approx 0.04$. Physical solutions must have $0 \leq f_{\mathrm{H}\alpha}^{(\mathrm{hot})} \leq 1$, $0 \leq f_{\mathrm{H}\alpha}^{(\mathrm{H\,I})} \leq 1$, and $0 \leq (1 - f_{\mathrm{H}\alpha}^{(\mathrm{hot})} - f_{\mathrm{H}\alpha}^{(\mathrm{H\,I})} - f_{\mathrm{H}\alpha}^{(\mathrm{refl})})$. Figure 5 shows one example, where the reflected H$\alpha$ fraction is set to 20%, $n(\mathrm{H}^+)/n_e = 0.5$ in the H I phase and $n(\mathrm{He}^+)/n(\mathrm{He}) = 0.3$ in the hot gas phase. The sensitivity to the first two parameters will be discussed below.

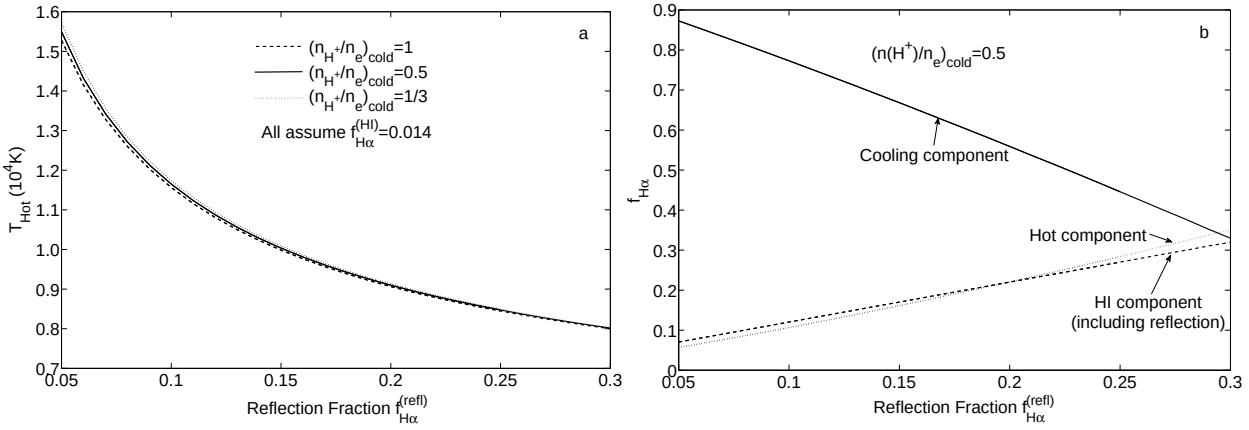


Fig. 6.— (a) Temperature $T_{\rm hot}$ and (b) fractional H$\alpha$ contributions from different ISM components, as functions of the reflected H$\alpha$ fraction $f_{\rm H\alpha}^{\rm (refl)}$, based on two constraints — $I_\nu(41\,{\rm GHz})/{\rm H}\alpha = 0.85\,{\rm kJy\,sr^{-1}R^{-1}}$ and [N II]$\lambda$6583/H$\alpha$ = 0.4 — for $f_{\rm H\alpha}^{\rm (refl)}$ ranging from 5% − 30%. It is assumed that only $f_{\rm H\alpha}^{\rm (H\,I)} \approx 0.014$ of the H$\alpha$ is emitted by the CNM and WNM components (see text). Panel (a) also shows the dependence of the solution ($T_{\rm hot}$) on the value of $n({\rm H}^+)/n_e$ in the H I gas. Our standard model assumes $\zeta_{\rm CR} = 1\times10^{-16}{\rm s}^{-1}$, which corresponds to $n({\rm H}^+)/n_e \approx 0.5$ in the "cold" phase, as discussed in Section 4.

In addition to the requirement that the fractions of all the three components have to be positive, which, for $f_{\rm H\alpha}^{\rm (refl)} \approx 0.2$, requires 8300$\leq T_{\rm hot} \leq$ 9800 K (see Figure 5), there is a second restriction coming from the fact that the total amount of H$\alpha$ emission from the H I phase is determined by the cosmic ray ionization rate. Consider a uniform layer of cold neutral gas with a column density $N$(HI), with cosmic ray ionization of H balanced by case B recombination as well as grain assisted recombination; the H$\alpha$ intensity from this component at latitude $b$ is

$$\frac{I_{\rm H\alpha}}{h\nu} = \frac{1}{4\pi}\frac{3\times10^{20}\,{\rm cm^{-2}}}{|\sin b|}\zeta_{\rm CR}(1+\phi_{\rm CR})\frac{\alpha_{\rm H\alpha}/\alpha_{\rm B}}{1+\alpha_{\rm gr}/x_e\alpha_{\rm B}} \quad , \tag{17}$$

where $x_e \equiv n_e/n_{\rm H}$, $\phi_{\rm CR} \sim 0.67$ is the number of secondary ionization per primary ionization in neutral gas (Dalgarno & McCray 1972), and $N({\rm HI}) \approx 3\times10^{20}|\sin b|^{-1}\,{\rm cm^{-2}}$ (Radhakrishnan et al. 1972; Dickey et al. 1978). Thus

$$\frac{I_{\rm H\alpha}}{h\nu} \approx \frac{0.01}{|\sin b|}\left(\frac{\zeta_{\rm CR}}{10^{-16}s^{-1}}\right){\rm R} \quad , \tag{18}$$

where the H I is taken to be a 1:1 mixture of CNM and WNM material.[1]

The distribution of H$\alpha$ for $|b| \geq 10^\circ$ has recently been measured by Hill et al. (2008), who found the full WIM to be fitted on average by $I_{\rm H\alpha}/h\nu \approx (0.625\pm0.002)|\sin b|^{-1}$ R. Comparing these two results, the fraction of H$\alpha$ *emitted* by the H I should only be $f_{\rm H\alpha}^{\rm (H\,I)} \approx 0.014(\zeta_{\rm CR}/10^{-16}{\rm s^{-1}})$.

[1]We have taken $\phi_{\rm CR} \approx 0.67$, $\alpha_{\rm H\alpha}/\alpha_{\rm B} \approx 0.6$, $\alpha_{\rm gr}/x_e\alpha_{\rm B} \approx 10$ for CNM with $T \approx 100\,{\rm K}$, $n_e \approx 0.01$, $n_{\rm H} \approx 30\,{\rm cm^{-3}}$ (Draine 2011); $\phi_{\rm CR} \approx 0.5$, $\alpha_{\rm H\alpha}/\alpha_{\rm B} \approx 0.5$ and $\alpha_{\rm gr}/x_e\alpha_{\rm B} \approx 0.5$ for $T \sim 5000$K WNM; and $N_{\rm CNM} \approx N_{\rm WNM} \approx \frac{1}{2}N_{\rm HI}$.

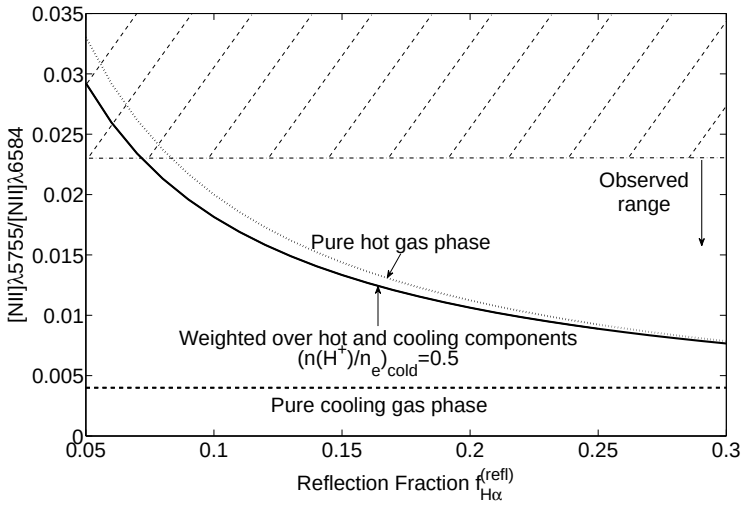


Fig. 7.— [N II]λ5755/[N II]λ6583 averaged over components (solid curve) as a function of reflection fraction based on the solution in panel (b) of Figure 7. Dashed curve and dotted curves show [N II]λ5755/[N II]λ6583 associated with pure cooling and pure hot gas phase, giving lower and upper limits of the ratio on individual sightlines. The result agrees with observations in Madsen et al. (2006), although comparison between the two is not straightforward (see discussion in Section 4).

In Figure 6 we take $f_{\rm H\alpha}^{\rm (H\,I)} = 0.014$ and consider different values of $f_{\rm H\alpha}^{\rm (refl)}$. For each $f_{\rm H\alpha}^{\rm (refl)}$, the H$\alpha$/free-free and [N II]/H$\alpha$ constraints serve to determine $f_{\rm H\alpha}^{\rm (hot)}$ and $T_{\rm hot}$, as shown in Figure 5. For $f_{\rm H\alpha}^{\rm (refl)}$ ranging from 5% to 30%, panel (a) in Figure 6 gives $T_{\rm hot}$ ranging from 8000–15000 K. For $f_{\rm H\alpha}^{\rm (refl)} = 0.2$, we find $T_{\rm hot} \approx 9100\,{\rm K}$.

One uncertainty when solving equations (15) and (16) is $n({\rm H}^+)/{\rm n_e}$ in the H I, which affects $\psi_{\rm H\,I}$ (equations 11). Assuming $\zeta_{\rm CR} \sim 10^{-16}{\rm s}^{-1}$, $T_{\rm CNM} \sim 10^2$ K and $n_{\rm CNM} \sim 30{\rm cm}^{-3}$, about half of the electrons come from metal elements, so the free-free/H$\alpha$ ratio for the H I will be $\Psi_{\rm HI} \approx 0.04$, as discussed in Section 2.2. We explore the effect of this uncertainty on $T_{\rm hot}$ in the range $0.02 - 0.06$, corresponding to $(n({\rm H}^+)/n_e)_{\rm cold} = 1$ and $\frac{1}{3}$, as shown in panel (a) of Figure 6. We find this uncertainty does not significantly affect the derived solutions.

In addition to [N II]λ6583/H$\alpha$, the [N II]λ5755/[N II]λ6583 ratio is another indicator of the temperature in the ionized medium. While [N II]λ6583 is one of the strongest lines in the WIM, comparable in intensity to H$\alpha$, [N II]λ5755 is extremely hard to detect due to its low intensity. Nevertheless, several measurements of this line ratio have been reported (Table 6 in Madsen et al. (2006)). The [N II]λ5755/[N II]λ6583 data have a large scatter, ranging from 0.023 (corresponding to a temperature over 12000 K) down to the observational upper limit 0.002 (corresponding to a temperature below 6000 K). In our WIM model the [N II]λ5755/[N II]λ6583 ratio is determined by the relative amounts of emission from the hot and cooling components, with the ratio for the cooling gas about 0.004 (almost model independent, as shown in Table 4). The solid curve in Figure 7 shows the weighted [N II]λ5755/[N II]λ6583 ratio based on the solutions in the panel (b) of Figure 6 for $f_{\rm H\alpha}^{\rm (refl)}$ ranging from 5%–30%, under the assumption that the [N II]λ5755/[N II]λ6583

ratio of the reflected light is the same as its value in the hot ionized gas, as we discussed previously. Note that this result is a *weighted average* value over all the components in the WIM – measurements along individual sightlines will vary. The observed [N II]$\lambda$5755/[N II]$\lambda$6583 value along a specific sightline depends on the weight of the three components along this sightline, which may differ from the weights that give the observed all sky averaged free-free to H$\alpha$ and [N II]$\lambda$6583 to H$\alpha$ ratio. The dashed curve and the dotted curve in Figure 7 show [N II]$\lambda$5755/[N II]$\lambda$6583 of the cooling gas and the hot gas, which could be interpreted as the lower and upper limit of the average [N II]$\lambda$5755/[N II]$\lambda$6583 value under extreme weighting cases. Nevertheless, the average weighted [N II]$\lambda$5755/[N II]$\lambda$6583 value ranges from 0.008 to 0.025, in general agreement with the observed values and upper limits in Madsen et al. (2006). Individual sightlines could have values of [N II]$\lambda$5755/[N II]$\lambda$6583 as low as 0.004, if the sightline is dominated by the cooling gas.

In sum, if the cooling gas is described by our standard model, the temperature of the hot gas and the fractions of the three components could be solved for so that a weighted sum of fractions of the three components:

1. reproduces the low observed free-free/H$\alpha$ ratio;
2. reproduces the observed [N II]$\lambda$6583/H$\alpha$ ratio
3. has [N II]$\lambda$5755/[N II]$\lambda$6583 in agreement with observations;
4. has a small fraction ($\sim$1.4%) of the H$\alpha$ *emitted* from H Igas;
5. includes a reflected component accounting for $\sim$20% of the total H$\alpha$

We emphasize again that the three-component model presented in this section is aimed to explain *averaged* observational results; individual sightlines will generally differ from the average because (1) the relative weights of its components differ from the average values, the temperature $T_{\rm hot}$ and the ionization conditions in the H II component may vary, and (3) the cooling component along an individual sightline may not be an average over the entire cooling and recombination. There is evidence that the physical conditions in the WIM do vary from sightline to sightline, and even among different velocity components within one sightline (Madsen et al. 2006). Different regions in the WIM will have different densities, cosmic ray ionization rates, elemental abundances, and histories. The three component model presented here is highly idealized, but it appears to provide a physical framework that is consistent with the observations.

## 5. Discussion

When the $h\nu > 13.6$ eV starlight is cut off at the beginning of the simulation, the hot gas begins to cool and recombine. The temperature, particle density and gas pressure decrease. In general, the cooling time scale is short, as shown in Figure 2: for $n_{\rm H} = 0.5$ cm$^{-3}$, $T$ falls below $10^3$ K within

0.3 Myr. If the photoionized gas was initially overpressured (relative to its surrounding), it would initially be expanding, resulting in adiabatic cooling after the photoionizing source turns off at $t = 0$. Conversely, if the photoionized gas was in pressure equilibrium with a confining medium at $t = 0$, it would begin to undergo compression as it cools and recombines at $t > 0$. However, if the $n_{\rm H} = 0.5\,{\rm cm}^{-3}$, photoionized region is $\sim$5 pc or larger, the cooling time will be short compared to the sound crossing time, and the effect of adiabatic expansion or compression should be of secondary importance. In the present work we assume isochoric evolution, which appears to be a reasonable approximation during the cooling phase.

In modeling the cooling gas, we assumed case B recombination. In the real WIM, some of the $h\nu > 13.6$ eV recombination radiation might escape from the WIM and get absorbed by nearby cold or warm neutral gas ($T \leq 1000$ K); the resulting ionized H in these cooler media would recombine, emitting H$\alpha$ and free-free emission, with a ratio of free-free emission to H$\alpha$ appropriate to $T \lesssim 1000$ K, lower than the ratio for the cooling gas. This would have the effect of decreasing the ratio of free-free emission to H$\alpha$ below the value calculated for the cooling gas model, allowing the observed low free-free/H$\alpha$ ratio to be explained by a somewhat smaller value of $f_{{\rm H}\alpha}^{\rm (cooling)}$, the fraction of the H$\alpha$ contributed by cooling and recombining gas. However, we expect this "escape" of ionizing photons to be minimal: the mean free path of $\sim$14 eV photons in partially recombined H is short, and we expect the case B on-the-spot treatment to be a valid approximation.

In our standard model, we choose $F_\star = 0$ for the elemental abundances in the WIM. In Jenkins' model, the nonzero initial depletion ($F_\star = 0$) is identified with the gas-phase abundances in a warm, low-density medium (Spitzer 1985; Savage & Sembach 1996), and should therefore apply to the WIM. Also, as mentioned above, there is evidence (DDF09) showing that the PAHs in the WIM are underabundant by a factor of $\sim$3. Our calculation shows that both factors are crucial for cooling the gas quickly enough and to a low enough temperature to be able to reproduce the observed low free-free/H$\alpha$ ratio. As shown in Figure 3, if there is no grain depletion or there is appreciable depletion of coolants (such as for $F_\star = 0.25$), the recombining gas stays relatively hot in the final steady state, and gives an unacceptable high integrated free-free/H$\alpha$ ratio.

Cosmic rays heat the gas directly, and they also raise the electron density $n_e$. If $n_e$ is low, photoelectron emission causes dust grains and PAHs to become positively charged, reducing the photoelectric heating rate. Thus increased cosmic ray ionization, by lowering the charge state of the dust and PAHs, has the effect of increasing the dust photoelectric heating rate. For our cooling gas model to be able to reproduce the low free-free/H$\alpha$ ratios that are observed, the ratio of cosmic ray primary ionization rate to gas density $\zeta_{\rm CR}/n_{\rm H}$ should not exceed $\sim 6\times10^{-16}\,{\rm cm}^3\,{\rm s}^{-1}$. For $\zeta_{\rm CR}/n_{\rm H} \gtrsim 5\times10^{-16}\,{\rm cm}^3\,{\rm s}^{-1}$ (e.g, $n_{\rm H} = 0.5\,{\rm cm}^{-3}$ and $\zeta_{\rm CR} = 5\times10^{-16}\,{\rm s}^{-1}$, with $\zeta_{\rm CR}/n_{\rm H} = 1\times10^{-15}\,{\rm cm}^3\,{\rm s}^{-1}$), the cosmic ray ionization maintains $n({\rm H}^+)/n_{\rm H} \geq 0.1$, and grain photoelectric heating can sustain the gas at $T \geq 10^3$ K. Observations of $H_3^+$ give estimates of $\zeta_{\rm CR} \approx (0.5-3)\times10^{-16}\,{\rm cm}^3\,{\rm s}^{-1}$, with an average of $\sim 2\times10^{-16}\,{\rm cm}^3\,{\rm s}^{-1}$ (Indriolo et al. 2007). If $\zeta_{\rm CR} \approx 2\times10^{-16}\,{\rm cm}^3\,{\rm s}^{-1}$, then the gas density cannot be much smaller than $n_{\rm H} = 0.5\,{\rm cm}^{-3}$ if the gas is to cool with $\Psi \leq 0.085$, as required to explain the low observed value of free-free/H $\alpha$. This high initial value of $n_e = 0.5\,{\rm cm}^{-3}$ seems

at first sight to be at odds with the study by Hill et al. (2008), which concluded that the most probable value of $n_e$ is only $n_e \approx 0.03\,\mathrm{cm}^{-3}$ in turbulent models of the WIM. Note, however, that in our standard model, the cooling gas ends up with $x_{\rm H} < 0.03$ and $n_e \approx 0.015\mathrm{cm}^{-3}$.

Because the observed line emission and free-free emission are weighted sums over 3 components, one of which (the cooling phase) itself has a range of temperature, there is no way to measure emission ratios associated with different phases unless the components could be separated. Temperatures derived from different line ratios need not agree. Moreover, even for a single line ratio, the contributions from different components may vary significantly from sightline to sightline, or with velocity on a single sightline. This may explain the large scatter in the physical conditions deduced from different line ratios.

The present model envisages intermittent photoionization events in the diffuse high-latitude gas, followed by cooling and recombination. Suppose that the probability per unit time of a photoionization event is $\tau_{\rm pi}$, with the ionizing radiation lasting a time $\tau_{\rm H\,II}$ before the photoionization switches off and the gas begins to cool and recombine. During the recombination phase, the number of H$\alpha$ photons per recombining $H^+$ is $\sim$0.5. The ratio of the H$\alpha$ emission from the photoionized gas to the emission from the cooling gas is

$$\frac{f_{\rm H\alpha}^{\rm (hot)}}{f_{\rm H\alpha}^{\rm (cooling)}} \approx \frac{\tau_{\rm pi}^{-1} \times n_e \alpha_{\rm H\alpha} \tau_{\rm H\,II}}{\tau_{\rm pi}^{-1} \times 0.5} \tag{19}$$

Hence,

$$\tau_{\rm H\,II} \approx \frac{0.5}{n_e \alpha_{\rm H\alpha}} \frac{f_{\rm H\alpha}^{\rm (hot)}}{f_{\rm H\alpha}^{\rm (cooling)}} \tag{20}$$

If $f_{\rm H\alpha}^{\rm (refl)} \approx 0.2$, then $f_{\rm H\alpha}^{\rm (hot)}/f_{\rm H\alpha}^{\rm (cooling)} \approx 0.22/0.56 \approx 0.39$, and the duration of the photoionization phase is only $\tau_{\rm H\,II} \approx 1 \times 10^5 (0.5\,\mathrm{cm}^{-3}/n_e)\,\mathrm{yr}$.

Given that O star lifetimes are $\sim 3 \times 10^6\,\mathrm{yr}$, such a short value of $\tau_{\rm H\,II}$ seems surprising. Longer values of $\tau_{\rm H\,II}$ can be obtained if $f_{\rm H\alpha}^{\rm (refl)}$ is larger: if $f_{\rm H\alpha}^{\rm (refl)} = 0.3$, then $f_{\rm H\alpha}^{\rm (hot)}/f_{\rm H\alpha}^{\rm (cooling)} \approx 0.35/0.33 \approx 1.1$, raising $\tau_{\rm H\,II}$ to $\sim 3 \times 10^5 (0.5\,\mathrm{cm}^{-3}/n_e)\,\mathrm{yr}$, but this is still short compared to O star lifetimes. Longer values of $\tau_{\rm H\,II}$ can be obtained if $n_e$ is lowered, but if $n_e$ is much smaller than $0.5\,\mathrm{cm}^{-3}$, grain photoelectric heating and cosmic ray heating prevent the gas from cooling to low enough temperature to be able to account for the observed low free-free/H$\alpha$ ratio, if, as assumed, the cooling takes place at $\sim$ constant density.

O star lifetimes are not the only time scale on which photoionization can vary. The ionizing radiation for the WIM may be provided in large part by *runaway* O and B stars, with space velocities $\gtrsim 100\,\mathrm{km\,s}^{-1}$. Modulation of the photoionization rate at a given point may result from motion of the ionizing sources through a medium of varying opacity: a star moving at $100\,\mathrm{km\,s}^{-1}$ travels 10 pc in $10^5$ yr.

Although O stars have been generally favored as the source of ionization for the WIM, it should be kept in mind that the actual source for WIM ionization has not been securely established.

According to the present analysis, the ionization phase, if it heats the plasma to $\sim 10^4$ K, needs to be of relatively short duration in order to be able to explain the low observed ratio of free-free/H$\alpha$. Perhaps other transient processes (such as shock waves or soft X-rays due to supernova blast waves, infalling gas, etc.) contribute to heating and ionization of the WIM.

A prediction of the current model is that the H$\alpha$ emission should have a component with the same radial velocity profile as the 21 cm emission, resulting from cosmic ray ionization of the H I. However, because cosmic ray ionization is thought to account for $\leq 2\%$ of the H$\alpha$, it may not be easy to recognize this component. The reflected component of H$\alpha$, [N II], etc, should also correlate with $N$(HI), but the apparent space velocities will differ from 21 cm radial velocities due to motion of the emitting H II relative to the reflecting dust grains.

## 6. Summary

The principal points of this paper are as follows:

1. We simulated the cooling and recombination of initially photoionized gas in the WIM following removal of $h\nu > 13.6$ eV radiation. The ratio of free-free emission to H$\alpha$, and emission line ratios such as [N II]$\lambda$6583/H$\alpha$, were calculated, and various factors which influence the cooling were explored. The result strongly depends on the abundances of elements, gas density, cosmic ray ionization rate, and the abundance of very small grains and PAHs, but depends only weakly on the initial temperature and ionization fractions, as shown in Figure 2, 3 and 4.

2. Based on these calculations, we propose a three component model — emission from hot ionized gas, cooling gas and neutral H I, plus reflected light – to explain multiple observations in the WIM. With plausible weighting factors for these components, the model *simultaneously* yields the low free-free to H$\alpha$ ratio, which indicates a low temperature ($\sim$3000 K, DDF09), and metal line ratios, such as [N II]$\lambda$6583/H$\alpha$ and [N II]$\lambda$5755/[N II]$\lambda$6583, which indicate a high temperature ($\sim 10^4$ K, Madsen et al. (2006)). The reflected component is crucial — there must be a fraction ($\sim$20%) of the observed H$\alpha$ coming from the reflected light, consistent with the estimate by Wood & Reynolds (1999), to explain the observation.

3. For our model to successfully reproduce the low free-free/H$\alpha$ ratio, some restrictions of the physical conditions in the WIM are required:

   (a) The ratio of cosmic ray primary ionization rate to gas density $\zeta_{\rm CR}/n_{\rm H}$ should not exceed $\sim 5 \times 10^{-16}{\rm cm^3 s^{-1}}$ (Figure 2), consistent with current observational estimates of $\zeta_{\rm CR}$ if $n_{\rm H} \approx 0.5{\rm cm^{-3}}$.

   (b) The gas phase element depletion parameter $F_\star \leq 0.25$ (Figure 3) so that there are sufficient gas phase coolants to cool the gas in the presence of heating by cosmic rays and photoelectrons from grains, consistent with Jenkins (2009).

(c) The abundance of ultrasmall grains (including PAHs) should be suppressed by a factor ∼3 relative to the abundances in the overall H I (Figure 3), consistent with DDF09.

4. Sightline-to-sightline variations of emission ratios are expected in our model. First, the parameters which affect the cooling model, such as the gas density, elemental abundances, cosmic ray ionization rate and the depletion factor of small grains, may vary spatially within the WIM. Second, different sightlines will have different proportions of the three components in our model. Third, the cooling component is time-dependent, and individual sightlines may not present a full average over the entire cooling history. These effects will lead to the variation of physical quantities deduced from observations on different sightlines, or for different velocity components on an individual sightline.

## Acknowledgments

We thank R. Benjamin for helpful discussions, and the anonymous referee for comments that led to improvements in the manuscript. This research was supported in part by NSF grants AST-0406883 and AST-1008570.

## REFERENCES

Abrahamsson, E., Krems, R. V., & Dalgarno, A. 2007, ApJ, 654, 1171

Arnaud, M., & Raymond, J. 1992, ApJ, 398, 394

Asplund, M., Grevesse, N., Sauval, A. J., & Scott, P. 2009, ARA&A, 47, 481

Bakes, E. L. O., & Tielens, A. G. G. M. 1994, ApJ, 427, 822

Baldwin, J. A., Ferland, G. J., Martin, P. G., Corbin, M. R., Cota, S. A., Peterson, B. M., & Slettebak, A. 1991, ApJ, 374, 580

Barinovs, Ğ., van Hemert, M. C., Krems, R., & Dalgarno, A. 2005, ApJ, 620, 537

Bautista, M. A., Quinet, P., Palmeri, P., Badnell, N. R., Dunn, J., & Arav, N. 2009, A&A, 508, 1527

Black, J. H., & van Dishoeck, E. F. 1991, ApJ, 369, L9

Collins, J. A., & Rand, R. J. 2001, ApJ, 551, 57

Dalgarno, A., & McCray, R. A. 1972, ARA&A, 10, 375

Davies, R. D., Dickinson, C., Banday, A. J., Jaffe, T. R., Górski, K. M., & Davis, R. J. 2006, MNRAS, 370, 1125

Dickey, J. M., Terzian, Y., & Salpeter, E. E. 1978, ApJS, 36, 77

Dobler, G., Draine, B., & Finkbeiner, D. P. 2009, ApJ, 699, 1374 (DDF09)

Dobler, G., & Finkbeiner, D. P. 2008, ApJ, 680, 1235

Draine, B. T. 1978, ApJS, 36, 595

—. 2011, Physics of the Interstellar and Intergalactic Medium (Princeton, NJ: Princeton University Press)

Ferguson, A. M. N., Wyse, R. F. G., Gallagher, III, J. S., & Hunter, D. A. 1996, AJ, 111, 2265

Ferrière, K. M. 2001, Reviews of Modern Physics, 73, 1031

Greenawalt, B., Walterbos, R. A. M., & Braun, R. 1997, ApJ, 483, 666

Griffin, D. C., Mitnik, D. M., & Badnell, N. R. 2001, J Phys B, 34, 4401

Haffner, L. M., et al. 2009, Reviews of Modern Physics, 81, 969

Haffner, L. M., Reynolds, R. J., & Tufte, S. L. 1999, ApJ, 523, 223

Hill, A. S., Benjamin, R. A., Kowal, G., Reynolds, R. J., Haffner, L. M., & Lazarian, A. 2008, ApJ, 686, 363

Hoopes, C. G., Walterbos, R. A. M., & Greenwalt, B. E. 1996, AJ, 112, 1429

Hoopes, C. G., Walterbos, R. A. M., & Rand, R. J. 1999, ApJ, 522, 669

Hudson, C. E., & Bell, K. L. 2005, A&A, 430, 725

Hummer, D. G. 1988, ApJ, 327, 477

Indriolo, N., Geballe, T. R., Oka, T., & McCall, B. J. 2007, ApJ, 671, 1736

Jenkins, E. B. 2009, ApJ, 700, 1299

Lepp, S. 1992, in IAU Symp. 150: Astrochemistry of Cosmic Phenomena, 471–475

Madsen, G. J., Reynolds, R. J., & Haffner, L. M. 2006, ApJ, 652, 401

Mathis, J. S., Mezger, P. G., & Panagia, N. 1983, A&A, 128, 212

McCall, B. J., et al. 2003, Nature, 422, 500

McKee, C. F. 1990, in Astronomical Society of the Pacific Conference Series, Vol. 12, The Evolution of the Interstellar Medium, ed. L. Blitz, 3–29

Miller, S. T., & Veilleux, S. 2003, ApJ, 592, 79

Nussbaumer, H., & Storey, P. J. 1986, A&AS, 64, 545

Otte, B., Gallagher, III, J. S., & Reynolds, R. J. 2002, ApJ, 572, 823

Pequignot, D. 1996, A&A, 313, 1026

Pequignot, D., Petitjean, P., & Boisson, C. 1991, A&A, 251, 680

Radhakrishnan, V., Murray, J. D., Lockhart, P., & Whittle, R. P. J. 1972, ApJS, 24, 15

Ramsbottom, C. A., Hudson, C. E., Norrington, P. H., & Scott, M. P. 2007, A&A, 475, 765

Rand, R. J. 1996, ApJ, 462, 712

—. 1997, ApJ, 474, 129

—. 2000, ApJ, 537, L13

Rand, R. J., Kulkarni, S. R., & Hester, J. J. 1990, ApJ, 352, L1

Reynolds, R. J. 1985, ApJ, 298, L27

Reynolds, R. J. 1991, in IAU Symposium, Vol. 144, The Interstellar Disk-Halo Connection in Galaxies, ed. H. Bloemen, 67–76

Reynolds, R. J. 1993, in American Institute of Physics Conference Series, Vol. 278, Back to the Galaxy, ed. S. S. Holt & F. Verter, 156–165

—. 2004, Advances in Space Research, 34, 27

Reynolds, R. J., Sterling, N. C., Haffner, L. M., & Tufte, S. L. 2001, ApJ, 548, L221

Rossa, J., & Dettmar, R. 2000, A&A, 359, 433

Savage, B. D., & Sembach, K. R. 1996, ARA&A, 34, 279

Sembach, K. R., Howk, J. C., Ryans, R. S. I., & Keenan, F. P. 2000, ApJ, 528, 310

Shull, J. M., & van Steenberg, M. 1982, ApJS, 48, 95

Sofia, U. J., & Parvathi, V. S. 2010, in Cosmic Dust – Near and Far, ed. T. Henning, E. Grün, & J. Steinacker, 236–242

Spitzer, Jr., L. 1985, ApJ, 290, L21

Stancil, P. C., Schultz, D. R., Kimura, M., Gu, J.-P., Hirsch, G., & Buenker, R. J. 1999, A&AS, 140, 225

Tayal, S. S. 2007, ApJS, 171, 331

—. 2008, A&A, 486, 629

Tayal, S. S., & Gupta, G. P. 1999, ApJ, 526, 544

Tayal, S. S., & Zatsarinny, O. 2010, ApJS, 188, 32

Verner, D. A. 1999, Subroutine rrfit, version 4, http:///www.pa.uky.edu/∼verner/fortran.html

Verner, D. A., & Ferland, G. J. 1996, ApJS, 103, 467

Verner, D. A., Ferland, G. J., Korista, K. T., & Yakovlev, D. G. 1996, ApJ, 465, 487

Verner, D. A., & Yakovlev, D. G. 1995, A&AS, 109, 125

Wang, J. Z., et al. 2002, ApJ, 564, 244

Webber, W. R., & Yushak, S. M. 1983, ApJ, 275, 391

Weingartner, J. C., & Draine, B. T. 2001a, ApJ, 563, 842

—. 2001b, ApJS, 134, 263

Wood, K., & Reynolds, R. J. 1999, ApJ, 525, 799

Table 3. Initial Ionization Fractions

| | | $IIF = 1$[a] | | | $IIF = 2$[b] | | | $IIF = 3$[c] | | | |
|---|---|---|---|---|---|---|---|---|---|---|---|
| $A$ | $n_A/n_{\rm H}$[d] | I | II | III | I | II | III | I | II | III | IV |
| H | 1 | 0.05 | 0.95 | ··· | 0.05 | 0.95 | ··· | 0 | 1 | ··· | ··· |
| He | 0.1 | 0.68 | 0.32 | 0 | 0.5 | 0.5 | 0 | 0.04 | 0.96 | 0 | ··· |
| C | $10^{-3.65}$ | 0.01 | 0.94 | 0.05 | 0.02 | 0.83 | 0.15 | 0 | 0.13 | 0.87 | 0 |
| N | $10^{-4.21}$ | 0.05 | 0.93 | 0.02 | 0.1 | 0.8 | 0.1 | 0 | 0.13 | 0.87 | 0 |
| O | $10^{-3.25}$ | 0.05 | 0.95 | 0.00 | 0.05 | 0.95 | 0.05 | 0 | 0.43 | 0.57 | 0 |
| Ne | $10^{-4.03}$ | 0.11 | 0.89 | 0.00 | 0.3 | 0.69 | 0.01 | 0 | 0.91 | 0.09 | 0 |
| Mg | $10^{-4.65}$ | 0.01 | 0.70 | 0.29 | 0.02 | 0.63 | 0.35 | 0 | 0.05 | 0.95 | 0 |
| Si | $10^{-4.61}$ | 0.00 | 0.87 | 0.12 | 0.01 | 0.74 | 0.25 | 0 | 0.05 | 0.83 | 0.12 |
| S | $10^{-4.58}$ | 0.00 | 0.78 | 0.22 | 0.02 | 0.68 | 0.3 | 0 | 0.03 | 0.95 | 0.02 |
| Ar | $10^{-5.56}$ | 0.01 | 0.76 | 0.23 | 0.15 | 0.75 | 0.1 | 0 | 0.11 | 0.89 | 0 |
| Fe | $10^{-5.41}$ | 0.00 | 0.34 | 0.64 | 0.01 | 0.69 | 0.3 | 0 | 0.01 | 0.24 | 0.75 |

[a]Standard Model in Sembach et al. (2000) with $\chi_{\rm edge} = 0.1$

[b]Estimate based on Haffner et al. (1999); Reynolds (2004); Madsen et al. (2006); Haffner et al. (2009); between IIF1 and IIF3

[c]Orion nebula values (Baldwin et al. 1991)

[d]Elemental abundance for standard Model ($F_\star = 0$)

Table 4. Models for Recombining Gas

| Name[a] | $n_{\rm H}$[b] ($cm^{-3}$) | $\zeta_{\rm CR}$[c] ($10^{-16}s^{-1}$) | $F_\star$[d] | g[e] | IIF[f] | $T_i$[g] ($K$) | $\Psi$[h] | $\Phi$[i] | $\frac{\rm [NII]\lambda5755}{\rm [NII]\lambda6583}$ [j] | $\frac{\rm [SII]\lambda6716}{\rm H\alpha}$ [k] |
|---|---|---|---|---|---|---|---|---|---|---|
| standard | 0.5 | 1.0 | 0 | 0.33 | 1 | 8000 | 0.081 | 0.060 | 0.0039 | 0.15 |
| $n_{\rm H} = 2.5$ | 2.5 | 1.0 | 0 | 0.33 | 1 | 8000 | 0.080 | 0.063 | 0.0039 | 0.16 |
| $n_{\rm H} = 2.5$ $\zeta_{\rm CR} = 0.2$ | 2.5 | 0.2 | 0 | 0.33 | 1 | 8000 | 0.080 | 0.063 | 0.0039 | 0.15 |
| $n_{\rm H} = 2.5$ $\zeta_{\rm CR} = 2.0$ | 2.5 | 2.0 | 0 | 0.33 | 1 | 8000 | 0.080 | 0.062 | 0.0039 | 0.15 |
| $n_{\rm H} = 2.5$ $\zeta_{\rm CR} = 3.0$ | 2.5 | 3.0 | 0 | 0.33 | 1 | 8000 | 0.079 | 0.062 | 0.0039 | 0.15 |
| $n_{\rm H} = 2.5$ $\zeta_{\rm CR} = 5.0$ | 2.5 | 5.0 | 0 | 0.33 | 1 | 8000 | 0.079 | 0.061 | 0.0039 | 0.15 |
| $\zeta_{\rm CR} = 0.2$ | 0.5 | 0.2 | 0 | 0.33 | 1 | 8000 | 0.081 | 0.062 | 0.0039 | 0.15 |
| $\zeta_{\rm CR} = 2.0$ | 0.5 | 2.0 | 0 | 0.33 | 1 | 8000 | 0.083 | 0.059 | 0.0039 | 0.15 |
| $\zeta_{\rm CR} = 3.0$ | 0.5 | 3.0 | 0 | 0.33 | 1 | 8000 | 0.088 | 0.060 | 0.0039 | 0.15 |
| $\zeta_{\rm CR} = 5.0$ | 0.5 | 5.0 | 0 | 0.33 | 1 | 8000 | 0.111 | 0.078 | 0.0032 | 0.42 |
| $F_\star = 0.25$ | 0.5 | 1.0 | 0.25 | 0.33 | 1 | 8000 | 0.099 | 0.085 | 0.0040 | 0.14 |
| Reduced C | 0.5 | 1.0 | 0+C[l] | 0.33 | 1 | 8000 | 0.088 | 0.065 | 0.0039 | 0.16 |
| $g = 1$ | 0.5 | 1.0 | 0 | 1.0 | 1 | 8000 | 0.109 | 0.083 | 0.0038 | 0.27 |
| $g = 0.1$ | 0.5 | 1.0 | 0 | 0.1 | 1 | 8000 | 0.075 | 0.056 | 0.0039 | 0.13 |
| IIF2 | 0.5 | 1.0 | 0 | 0.33 | 2 | 8000 | 0.083 | 0.054 | 0.0038 | 0.14 |
| IIF3 | 0.5 | 1.0 | 0 | 0.33 | 3 | 8000 | 0.083 | 0.028 | 0.0028 | 0.063 |
| $T_i = 10^4$ K | 0.5 | 1.0 | 0 | 0.33 | 1 | 10000 | 0.086 | 0.099 | 0.0069 | 0.23 |

[a]Model name

[b]H nucleon density

[c]Cosmic ray primary ionization rate.

[d]Depletion parameter from (Jenkins 2009)

[e]The grain reduction factor. The grain assisted recombination rate and photoelectric heating rate reduce to this fraction of their full values.

[f]Initial ionization fractions (see Table 3)

[g]Initial gas temperature.

[h]Integrated ratio of free-free at 41 GHz to H$\alpha$, as in Equation 11, for $n_{\rm H}t = 10^7{\rm cm}^{-3}{\rm yr}$.

[i]Integrated ratio of [NII] $\lambda$6583 to H$\alpha$, as in Equation 14, for $n_{\rm H}t = 10^7{\rm cm}^{-3}{\rm yr}$.

[j]Integrated ratio of [NII] $\lambda$5755 to [NII] $\lambda$6583, for $n_{\rm H}t = 10^7{\rm cm}^{-3}{\rm yr}$.

[k]Integrated ratio of [SII] $\lambda$6716 to H$\alpha$, for $n_{\rm H}t = 10^7{\rm cm}^{-3}{\rm yr}$.

[l]Element abundance identical to the standard model ($F_\star = 0$) except for C, for which we take the $F_\star = 0$ value $\times(2/3)$, or $n_{\rm C}/n_{\rm H} = 1.4 \times 10^{-3}$